SUPPORTING ONLINE MATERIAL

For the manuscript: **Direct observation of stalled fork restart via fork regression in the T4 replication system**

This supplement contains:

Materials and Methods

Supporting Figures S1 – S19

Supporting References 20-28

Materials and methods

Proteins and buffer

The T4 proteins, full-length UvsW (11), ATPase-deficient active site mutant K141R (13, 20), gp43 polymerase (21), gp45 processivity clamp (22), gp44/62 clamp-loader complex (23), gp41 helicase (24), and gp32 single-stranded DNA-binding protein (25) were purified as previously described. Experiments were performed in replication buffer containing 25 mM TrisOAc (pH 7.50), 150 mM KOAc, 10 mM MgOAc, 1 mM DTT and 1 mM ATP. In the experiment where the effect of ATP on the annealing activity of UvsW was examined (fig. S6), ATP was varied from 0.01 – 1 mM. In single-molecule lesion bypass and competition assays (Fig.3, fig. S14, S16 and S17) we used 2.5 mM of ATP and 100 μM of dNTPs. Both ensemble experiments and single-molecule experiments were performed at 37 ºC. Protein concentration in single molecule assays were: 10 nM UvsW (60 nM in experiments presented in figs. S4 and S7 and 3nM in experiments presented in fig. S11), 10 nM gp43, 30 nM gp45, 10 nM gp4462, 50 nM gp41, 300 nM gp32.

DNA substrates for Single Molecule Measurements.

The Mh 1.2 Kbp and Lh 7 Kbp DNA hairpin substrates were constructed as previously described (26, 27). Similarly, a 100 bp short DNA hairpin substrate (Sh) containing three locked nucleic acid (LNA) nucleotides to inhibit the polymerization reaction of the holoenzyme was constructed (fig. S2A). Briefly, a fork structure formed by two partially annealed oligonucleotides (A-1 was 5′-biotinylated to allow for attachment to the magnetic bead and A-3) and a short hairpin oligonucleotide (C) were annealed and ligated to the compatible ends of an 80 bp DNA fragment formed by annealed oligonucleotides (B-1 and B-2), fig. S1A; oligonucleotide sequences are given in Table S1. The digoxigenin label was incorporated by annealing a primer (oligo A-2) to the template strand and filling in the overhang with Klenow Fragment (3′ → 5′ exo$^-$) (New England Biolabs) in the presence of dUTP-digoxigenin (Roche). The hairpin products were purified with NucleoSpin Extract II Kits (Clontech). The mechanical stability of the DNA hairpin constructs was characterized by measuring the extension of the substrate as a function of the pulling force along a force-cycle in which the force was first increased and then relaxed (fig. S2C,E,F). We observed stably folded hairpin substrates below ~10 pN and mechanical unfolding of the hairpins above ~ 16 pN. Fork

substrates for single-molecule branch migration assays and lesion bypass assays were generated in situ in the reaction chamber as described in figs. S10A and S12.

Magnetic Tweezers assays

We used a PicoTwist magnetic tweezers instrument (www.picotwist.com) to manipulate individual DNA hairpin molecules tethered between a glass surface at the 3′ end and a magnetic bead at the 5′ end (fig. S2B). The glass surface was treated with anti-digoxigenin antibody (Roche) and passivated with bovine serum albumin (BSA). Streptavidin-coated Dynal magnetic beads (Invitrogen) were 1 μm in diameter. The DNA hairpins were manipulated by capturing the bead in a magnetic trap generated by a pair of permanent magnets. The applied force was controlled by varying the distance of the magnets from the sample. Video-microscopy was used to track the position of the magnetic bead in three dimensions with nanometer resolution at 30 Hz, from which the extension of the DNA molecule and the strength of the stretching force were deduced (12). A calibration curve of the applied force versus the vertical position of the magnets was used to exert forces within 10% error on the DNA molecules.

Single-molecule data analysis

Raw data, corresponding to the real-time evolution of the DNA extension in nm, was converted into the number of base pairs annealed or base pairs migrated by UvsW using a calibration factor determined from the elastic properties of ssDNA and dsDNA (fig. S3). Instantaneous enzymatic rates were obtained from a linear fit to the traces filtered with a third-order Savitzky-Golay filter over a time window of 0.1s. The histogram of the instantaneous rates was fit to Gaussian functions. The error bars shown in the histograms are proportional to the inverse of the square root of the number of points for each individual bin.

FRET based ensemble annealing assay.

The FRET based ensemble assay for determining the kinetics of annealing of complementary ssDNA involved the use of two types of substrates, when annealed they would generate partial duplex DNA structures with a 3′-tail carrying the FRET pair either at the duplex end or at the junction of the dsDNA/ssDNA. The ssDNA substrates with the following sequence 5′-Cy5-AGAGTACGAGGATACTTGAATACG-3′ and 5′-CGTATTCAAGTATCCTCGTACTC - Cy3-GTACTGACTCCGATCCGACTGTCC-3′

were used in the FRET assay that involves the generation of a partial duplex DNA with a FRET pair at the dsDNA/ssDNA junction. The oligonucleotides with the sequences 5′-ACAGAGTACGAGGTATCTTGAATACGTTA-Cy5-3′ and 5′-Cy3-TAACGTATTCAAGATACCTCG TACTCTGTACTGACTCCGATCCGACTG-3′ were employed for the duplex with the terminal FRET pair bearing duplex DNA structures.

In the ensemble annealing assay, the two complementary strands (3 nM), each carrying either a Cy3 or Cy5 dye, were mixed in the presence of 10-fold excess of UvsW (30 nM). The assay mixture was excited at 532 nm and the kinetics of annealing were followed by monitoring the increase in the Cy5 signal at 675 nm due to the FRET between the two dyes upon annealing of the two complementary strands catalyzed by the UvsW helicase. The data thus obtained under pseudo first-order conditions were then fit to a single exponential equation (1) to obtain the rate constant for enzyme-catalyzed annealing under ensemble conditions. The spontaneous annealing reaction was carried out by excluding the enzyme in the assay mixture. Another control reaction where ATP was replaced by a slowly hydrolysable analog ATPγS was also carried out. The data thus obtained are shown in fig. S5.

$$F = A_1 \exp(-k_1 t) + C \qquad (1)$$

UvsW mediated unwinding of a synthetic HJ substrate using a radiometric assay.

Synthetic HJ substrate for ensemble unwinding assay was generated employing the following oligonucleotides:
5′ACGCTGCCGAATTCTGGCTTGCTAAAGGATAGGTCGAATTTCTCATTTT-3′,
5′-CAAAGTAAGAGCTTCTCGAGCTGCGCTAGCAAGCCAGAATTCGGCAGC

GT-3′, 5′-TCTTTGCCCAAATGCAGGTTCACCCGCGCAGCTCGAGAAGCTCTT

ACTTTG-3′ and 5′-AAAATGAGAAAATTCGACCTATCCTTGGGTGAACCT

GCATTTGGGCAAAGA-3′. Here the synthetic branched HJ substrate composed of four complementary oligonucleotides, where one of the strands was radiolabeled with ^{32}P and, these complementary strands were annealed to generate a HJ substrate (13). This substrate was employed to measure the kinetics of the HJ unwinding activity of

UvsW. The reaction was initiated by the addition of 30 nM of UvsW to a pre-incubated mixture of the HJ substrate in the reaction buffer with 2 mM ATP containing an ATP-regeneration system. The reaction was quenched with a buffer containing 50 mM EDTA, Proteinase K, and unlabeled primer trap at various time points and the products of the unwinding assay were resolved on a native PAGE gel. The data thus obtained is shown in fig. S9.

Table S1. Oligonucleotides (Eurogentec and Integrated DNA technology) used to construct the short DNA hairpin (Sh). LNA modified bases are indicated in red.

A-1	5′-biotin-TTT TTT TTT TTT TTT TTT TTT TTT TTT TTT TTT TTT TTT TTT TTT TTT TTT TTG GAT TCG CGG GTC TCT-3′
A-2	5′-AAC CGT CCT TTA CTT GTC ATG CGC TCT AAT CTC TGG GCA TCT GGC TAT GAT GTT GAT GGA ACT GAC CAA ACG TCG GTG GG-3′
A-3	5′-phosphorylated-AGG AAG AGA CCC GCG AAT CCC CCA CCG ACG TTT GGT CAG TT-3′
B-1	5′-phosphorylated-TCC TGA TTG TCA TCG GCT GGC TGT TCG GTT AGT TTC GAA GAC TT-3′
B-2	5′-phosphorylated-GCG AAA GTC TTC GAA ACT AAC CGA ACA GCC AGC CGA TGA CAA TC-3′
C	5′-phosphorylated- TCG CGG AGT ATA ACA TTG ATA TCA ATC AAA TGT TGA ATA TGT TCT AGT TTT TTC TAG AAC ATA TTC AAC ATT TGA TTG ATA TCA ATG TTA TAC TCC-3′

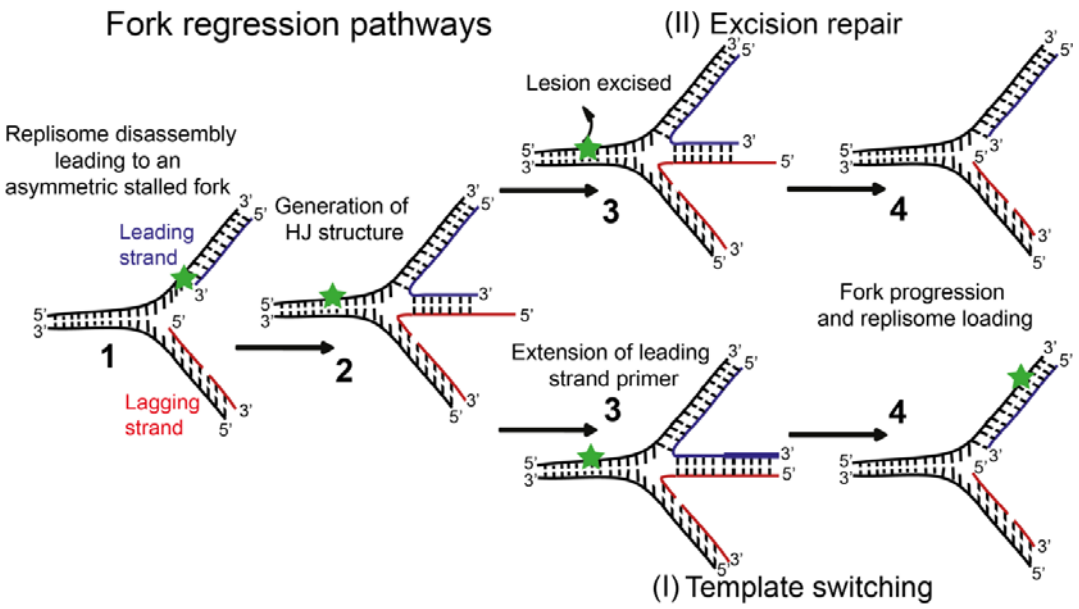

Fig. S1: Fork regression pathways for reactivating forks that have been stalled by leading strand lesions: (I) template switching and (II) excision repair. The DNA lesion on the leading strand is shown as a star (green). The nascent strands from the leading and lagging strand DNA synthesis are shown in blue and red respectively.

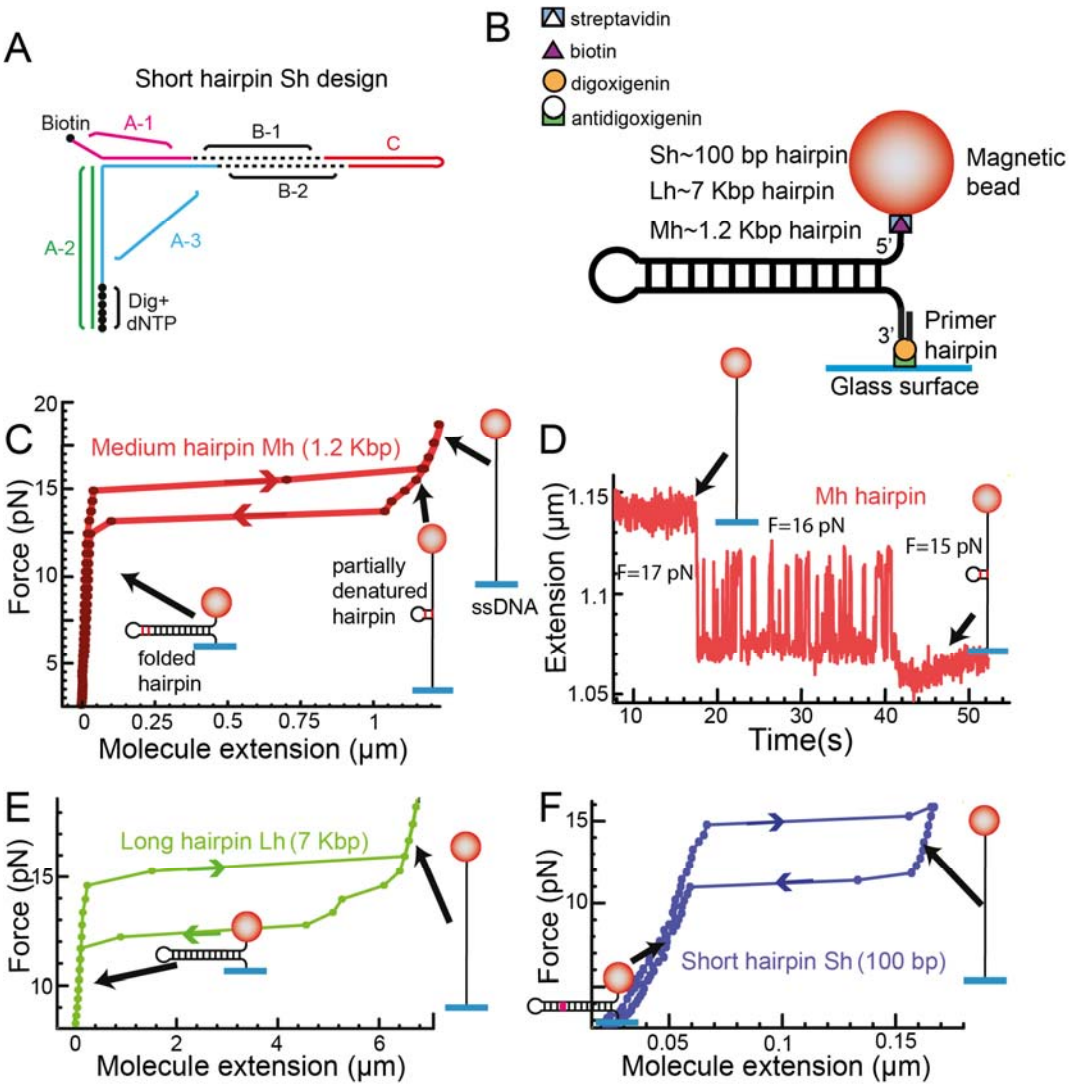

Fig. S2: DNA hairpin constructs and their mechanical properties. (**A**) Schematic representation of the short DNA hairpin substrate (Sh). (**B**) Schematic representation of a DNA hairpin with a built-in primer tethered between a magnetic bead and the glass surface. (**C**) Force-extension curve for the Mh (1.2 Kbp) hairpin demonstrating stable hairpin folding and constant extension as the applied force was increased to ~15 pN, at which point the extension abruptly increased due to the mechanical unfolding of the hairpin, followed by rapid re-annealing and return to its initial extension when the applied force was decreased below ~12 pN. (**D**) Trace showing the molecular extension of the Mh substrate at three forces. At 17 pN the hairpin is fully opened. At 16 pN the molecule hops between the fully opened (i.e. completely denatured) and partially denatured hairpin configurations, detected as jumps in the measured molecular

extension. At 15 pN the molecule is stable at the partially denatured hairpin configuration. (**E**) Force-extension curve for the Lh (7 Kbp) hairpin. (**F**) Force-extension curve for the Sh (100 bp) hairpin.

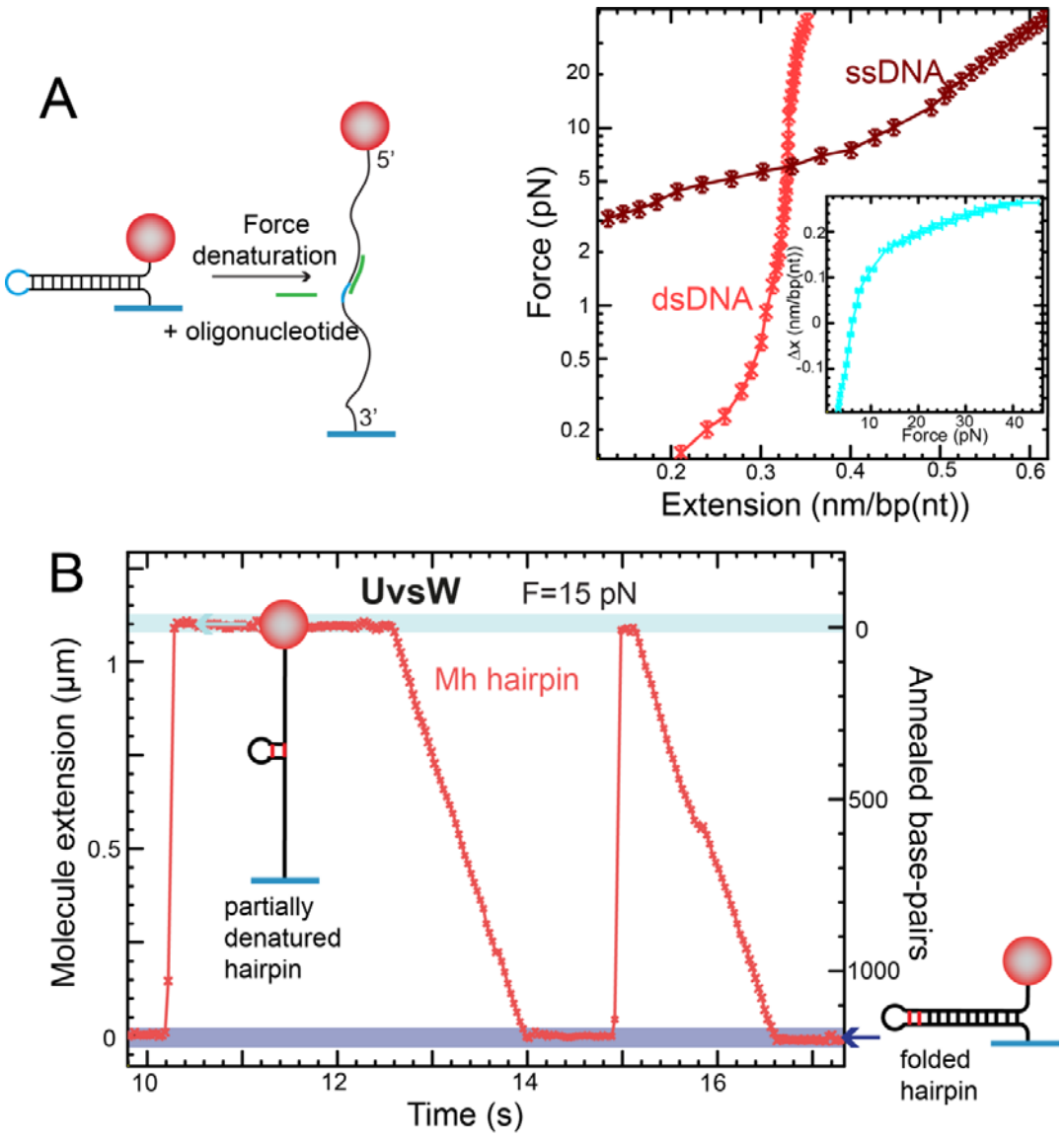

Fig. S3: Measurement of ssDNA and dsDNA elasticity and calibration factors. (**A**) The ssDNA elasticity was measured using the Mh substrate in the presence of a 20-mer oligonucleotide complementary to the loop region of the hairpin. The Mh substrate was mechanically opened by applying a 20 pN force in the presence of 1 μM oligonucleotide allowing the hybridization of the oligonucleotide (left panel). The hybridization of the oligonucleotide generated a large (several k_BT) kinetic barrier to hairpin re-annealing permitting the force-extension curve for ssDNA (dark red) to be measured (right panel). The dsDNA elasticity (light red) was measured following replication of the entire hairpin (right panel). (**B**) Experimental trace showing the annealing activity of UvsW at 15 pN with the Mh partially denatured hairpin. The ssDNA elasticity was used to

compute the conversion factor between the measured extension change and number of annealed base-pairs (right axis).

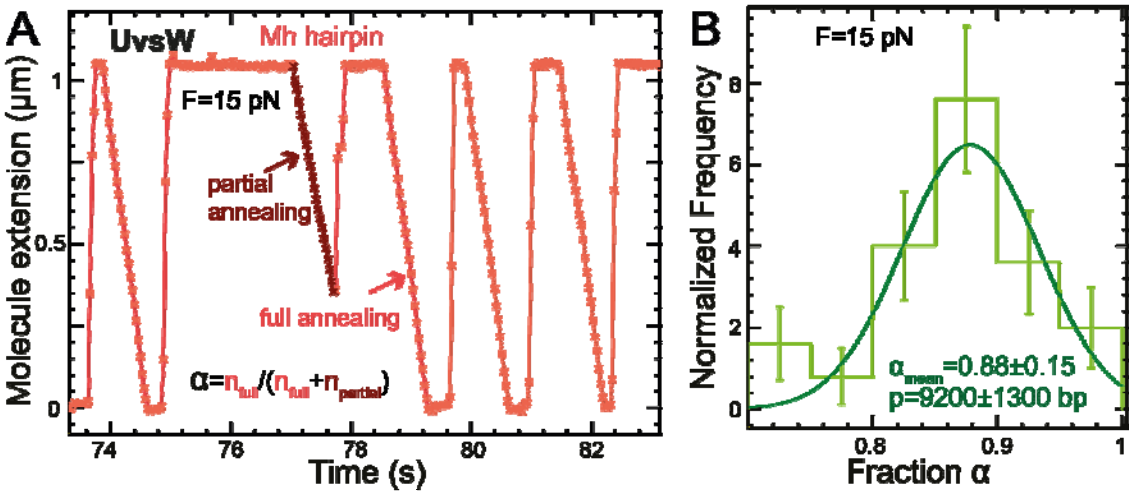

Fig. S4: Measurement of the UvsW processivity. (**A**) Experimental trace showing the UvsW annealing activity on the Mh partially denatured hairpin at 15 pN and at high protein concentration (60 nM). Most of traces show full annealing events corresponding to the annealing of the complete hairpin. For a given trace, the fraction α is computed as the ratio between the number of full annealing events and the total number of events. (**B**) Distribution of the fraction of full annealing events α (from 43 independent experiments, analyzing N=766 events). The fit to a Gaussian function is shown as a continuous line. Assuming that enzyme dissociation can be described as a Poisson process, the processivity p was computed as $p = -m/\ln(\alpha_{mean})$, where m is the number of base-pairs unwound at the initial configuration (m~1200 bp). This led to an estimate for the processivity of ~9000 bp.

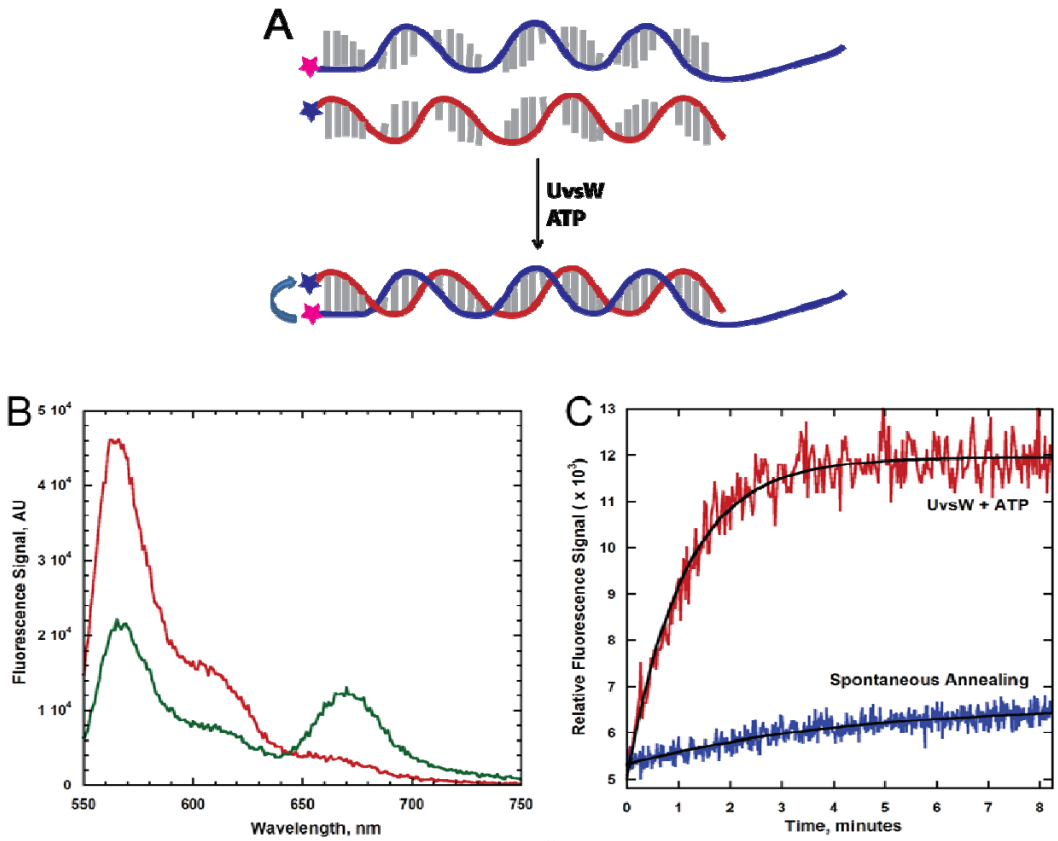

Fig. S5: Annealing activity of UvsW measured by an ensemble FRET-based assay. **(A)** Annealing activity of UvsW measured employing ssDNA where one of the ssDNA substrates carried a FRET donor (Cy3) while the other carried a FRET acceptor (Cy5). (**B**) The annealing activity was measured by exciting the donor and following the acceptor fluorescence increase with time. The emission spectrum of Cy3 bearing DNA (3 nM) excited at 514 nm with a maximum peak at 565 nm (red). The emission spectrum of Cy3 DNA and Cy5 DNA (3 nM), UvsW (30 nM) and ATP (4 mM) incubated for 5 min (green). The enzyme mediated annealing can be confirmed from the FRET between the Cy3 and Cy5 with a drop in the Cy3 emission and a concomitant increase in the signal for the Cy5 emission after annealing of the strands. (**C**) The data obtained from the assay under pseudo first-order conditions were then fit to a single exponential equation to obtain the rate constant for enzyme-catalyzed annealing under ensemble conditions of 0.92 ± 0.02 min^{-1}.The spontaneous annealing of the ssDNA obtained by excluding the enzyme yielded a rate constant of 0.20 ± 0.02 min^{-1}.

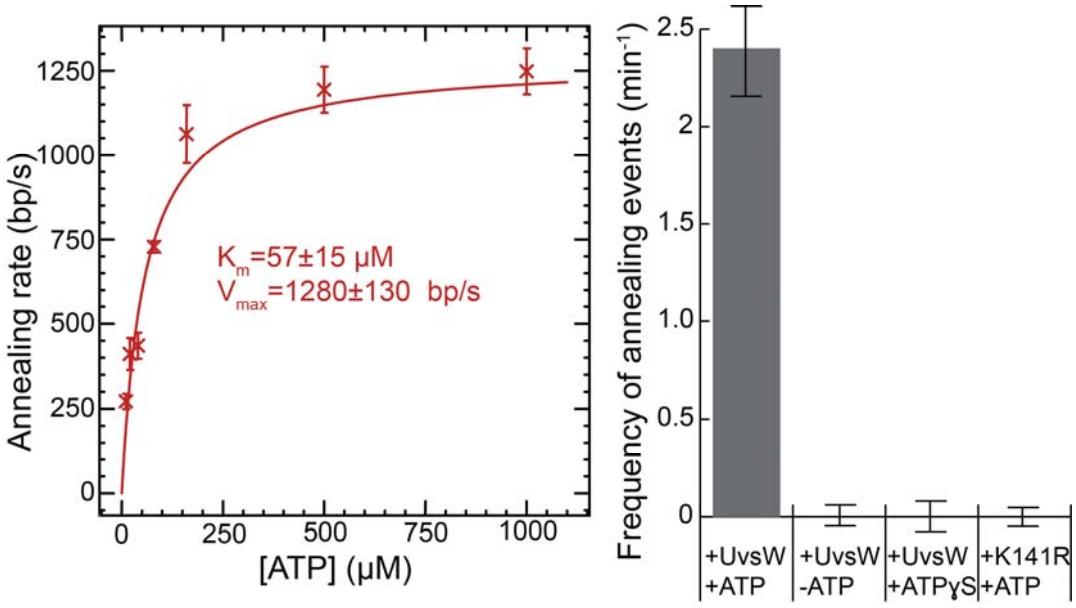

Fig. S6: UvsW anneals DNA in an ATP hydrolysis-dependent manner (**A**) Mean annealing rate as a function of the ATP concentration measured in the MT annealing assays with the Mh partially denatured hairpin at 15 pN of applied force. Fitting the data to a hyperbolic saturation equation (continuous line), taking into account the error in data, a K_M and k_{cat} of 57 μM and 1280 bp/s, were obtained with χ^2 =6 (computed from N=52 to 256 events depending on the ATP concentration). Error bars are the SEM. (**B**) Frequency of annealing events measured in experiments with UvsW and an ATPase-deficient active site mutant K141R with different nucleotide conditions (ATP, ATPγS and no ATP), computed from 31 to 63 independent experiments depending on the conditions. Error bars are the SEM. In absence of ATP or presence of ATPγS, no annealing activity was detected in our assays with the full-length UvsW protein. Likewise, the ATPase-deficient active site mutant K141R did not show any annealing activity. These observations revealed that ATP hydrolysis was necessary for the annealing activity of the UvsW enzyme.

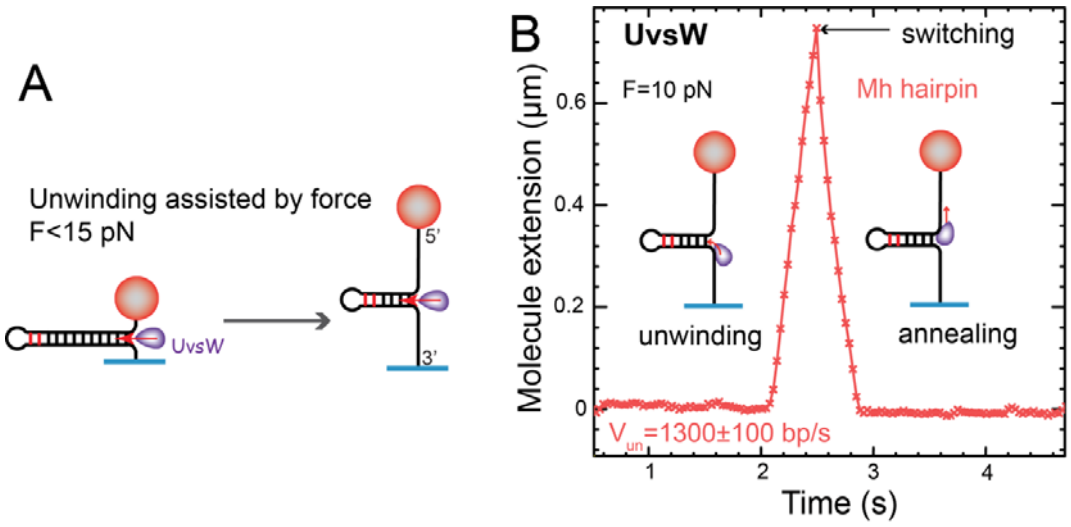

Fig. S7: UvsW single molecule unwinding assays (**A**) Schematics of the MT unwinding assay. Unwinding could be investigated at forces below 15 pN, a situation in which the hairpin structure was stable and annealing was prevented. The unwinding activity of the helicase could be detected as an increase in the molecular extension. (**B**) Experimental trace showing the molecular extension as a function of time obtained in the MT with the Mh hairpin. Unwinding was studied at applied forces ranging from 5-13 pN, well below the unfolding force of 15 pN. The trace presented corresponds to an experiment at 10 pN. At the conditions studied, UvsW unwinding activity on the Mh hairpin was very rare. Just very few events were observed (four events detected tracking ~30 beads during several hours), even at high UvsW concentration (60 nM). Moreover, when unwinding occurred, it did not proceed until the end of the hairpin. In contrast, the enzyme switched from unwinding to annealing activity after a few hundreds of base-pairs. The number of unwound or annealed base-pairs was deduced by using the elastic properties of ssDNA measured independently (fig. S3). The measured average unwinding rate was 1300 bp/s in agreement with the measured annealing rate.

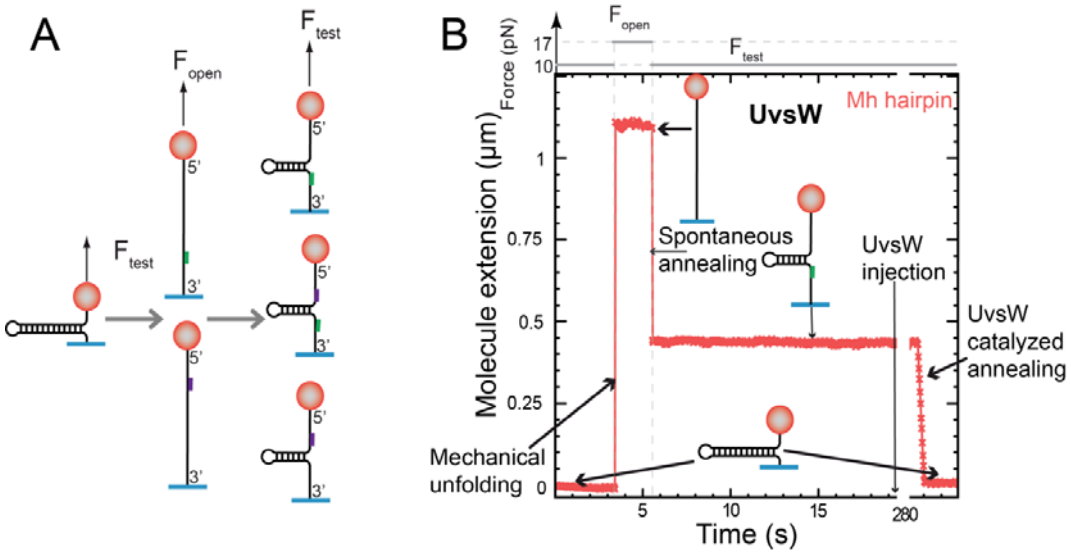

Fig. S8: UvsW simultaneous unwinding and annealing activities to resolve DNA branch structures. (**A**) Schematics of the branched substrate constructions generated in situ in the reaction chamber. By mechanically denaturing the Mh hairpin and flowing into the chamber a 90-mer oligonucleotide complementary to a central region of the hairpin, a shorter hairpin was generated with long ssDNA tails containing a short dsDNA region at the junction between the dsDNA hairpin and the 3′ or/and 5′ tail. This substrate was then used to test the ability of UvsW to resolve branch structures. (**B**) Experimental trace showing the UvsW annealing activity on the partially denatured hairpin with an oligonucleotide hybridized on the leading strand. The force was first increased to 17 pN to denaturate the hairpin and next relaxed to 10 pN to generate the partially denatured hairpin. UvsW annealed the hairpin by expelling the hybridized oligonucleotide. We obtained the same annealing results when a single oligonucleotide was hybridized on the lagging strand or when two oligonucleotides were used (one hybridized in each strand). In these assays hairpin unwinding (as observed when annealing is prevented, fig. S7) was never observed. Therefore, UvsW clearly presented a much stronger annealing activity over unwinding activity and the preference for annealing activity was independent of the location of the oligonucleotide on the ssDNA under the conditions employed for these experiments.

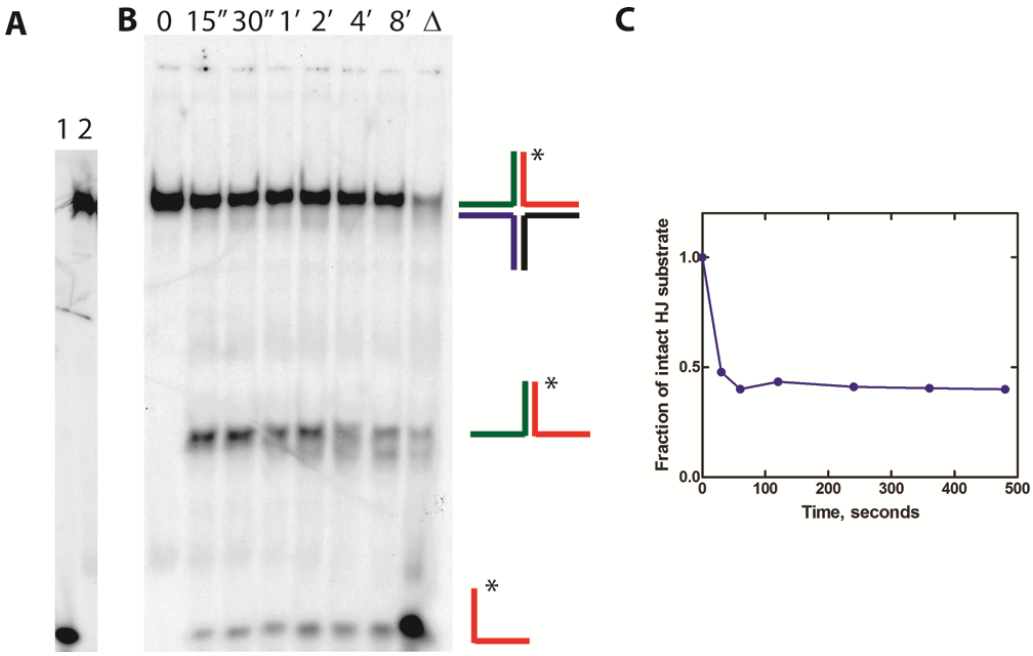

Fig. S9: Ensemble HJ unwinding activity of UvsW helicase. (**A**) Generation of synthetic Holliday junction substrate. Intact HJ substrate (lane 2) and Unwound Holliday junction by heating to 95 ºC (lane 1). (**B**) Kinetics of UvsW catalyzed unwinding of HJ structures employing a simple synthetic branched HJ substrate composed of four complementary oligonucleotides where one of the strands was radiolabeled with ^{32}P. When these four strands were heated and gradually cooled to room temperature, a HJ substrate was generated. This substrate was employed to measure the kinetics of HJ unwinding activity of UvsW. The reaction was initiated by the addition of 30 nM enzyme to the substrate (130 nM) in reaction buffer containing 2 mM ATP, quenched with a buffer containing 50 mM EDTA, Proteinase K, 500 nM unlabeled primer at various time points (15 s to 8 min) and the products were resolved on a native PAGE gel. The results showed that the HJ unwinding is catalyzed by UvsW in a time-dependent manner. The initial product of unwinding in turns is a substrate for UvsW that is also unwound in a time-dependent manner. (**C**) The PAGE gel was quantified using ImageQuant and the results of the unwinding are shown. At high concentrations of UvsW, 200 nM, the HJ substrate is unwound completely instantaneously. Hence the concentrations were lowered to follow the time-dependence of HJ unwinding.

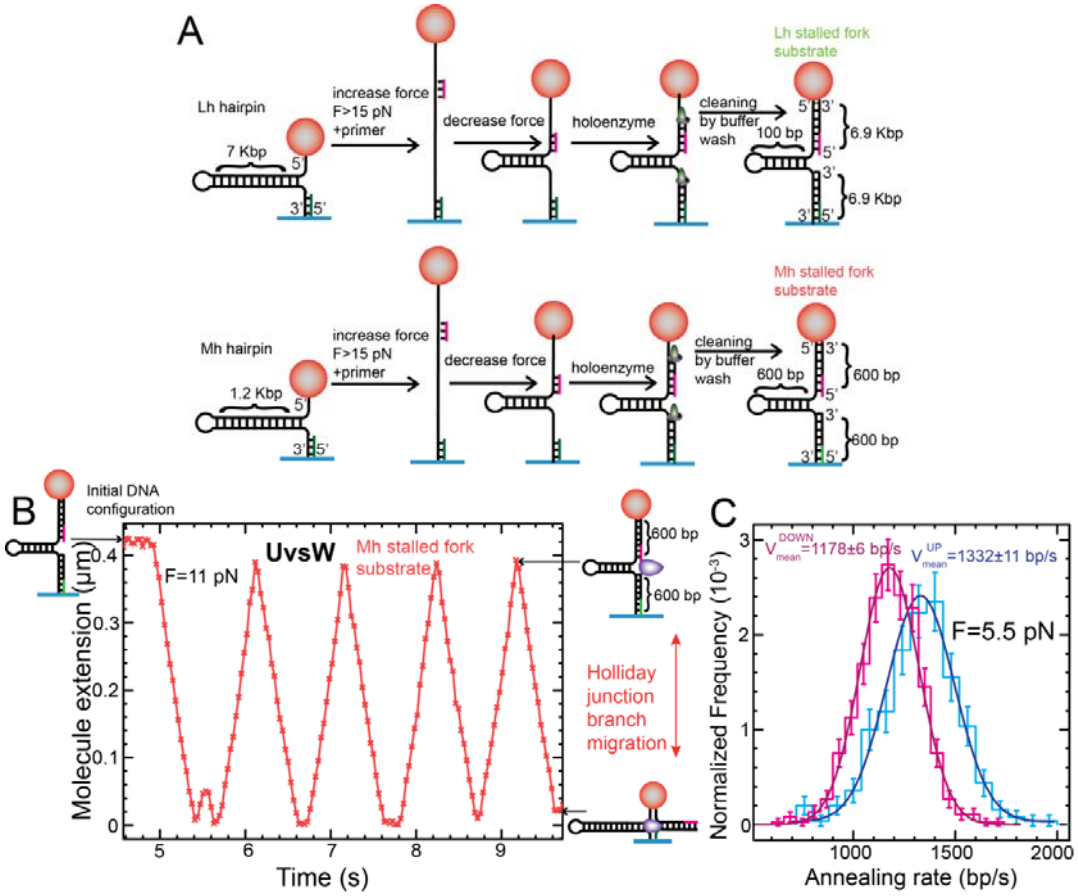

Fig. S10: Single molecule HJ migration assays (**A**) Schematics of the stalled fork substrate constructions generated in situ in the reaction chamber. By mechanically denaturing the 7 Kbp (Lh) or the 1.2 Kbp (Mh) hairpin with a built-in primer and flowing an 90-mer oligonucleotide into the chamber we built a partially denatured hairpin with primers hybridized in both leading and lagging strands. The two primers were next extended by the T4 holoenzyme complex (composed of the polymerase gp43 and the processivity clamp gp45 (14)) whose strand displacement activity could be controlled by the applied force (forces < 6 pN inhibit synthesis) (15). Since the force applied was low (4 pN), the polymerization in the leading strand stopped upon encountering the duplex region of the hairpin and we ended up with a replication fork-like-substrate. (**B**) Experimental trace showing the molecular extension as a function of time obtained from the HJ migration assays using the Mh stalled fork. HJ migration was studied at applied forces ranging from 2-11 pN. At this range of forces (well below the unfolding force of the hairpin, ~15 pN) the hairpin is mechanically stable and the fork is

fomed. The trace presented corresponds to an experiment at 11 pN. (**C**) Distribution of HJ migration rates measured in the downward and upward directions (N=536 events) with Gaussian fit (continuous lines) at 5.5 pN of applied force.

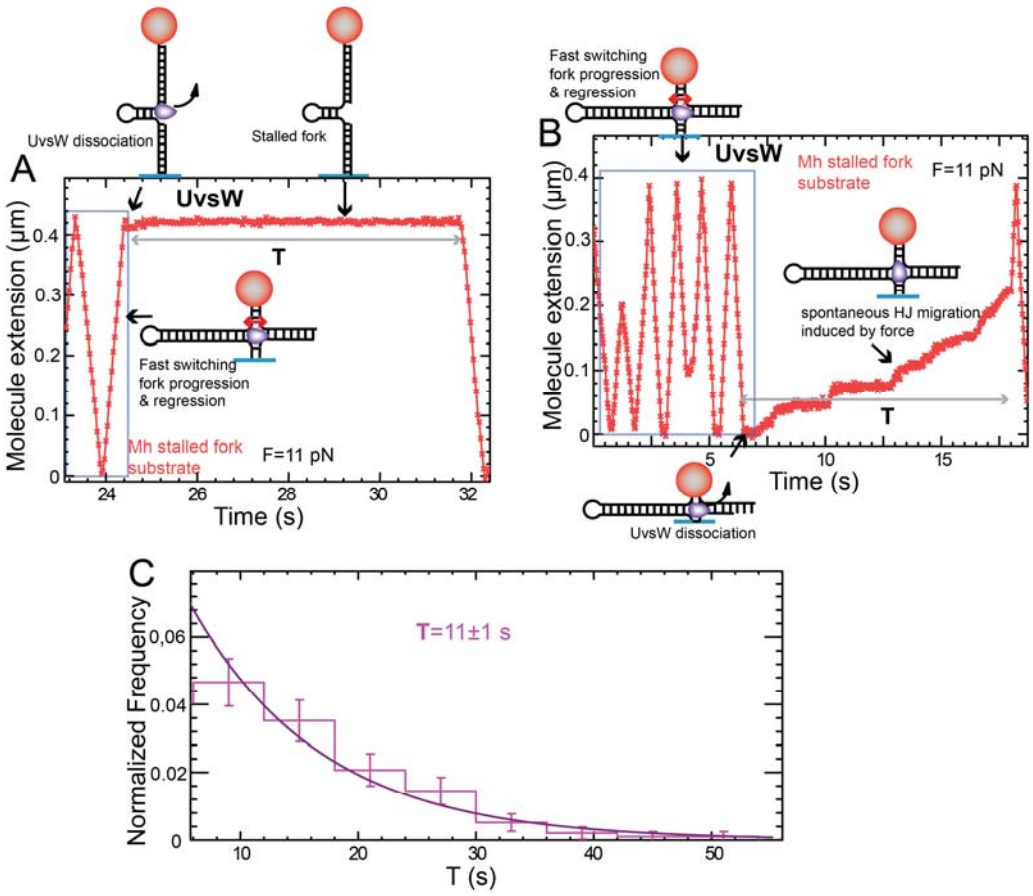

Fig. S11: Instantaneous switches in the branch migration direction are not generated by the loading of new UvsW molecules from solution (**A, B**) Experimental traces showing the molecular extension as a function of time obtained from the HJ migration assays using the Mh stalled fork at F=11 pN. In panel A, instantaneous switches in the migration direction were observed until the enzyme dissociated after the fork had been restored. The molecular extension remained constant for about ~8 s before another enzyme loaded and started the fork regression reaction. In panel B, the enzyme dissociation occurred after the fork had been totally regressed. The slow increase in the molecular extension corresponded to the spontaneous HJ migration, not catalyzed by UvsW but induced by the force applied. After ~10 s, fast HJ migration was observed again due to UvsW reloading. (**C**) Distribution of the characteristic time lag τ between fast HJ migration activity bursts catalyzed by UvsW (N=108 events). The fit to an exponential function is shown as a continuous line. The characteristic time lag τ (11 s) is much larger than the time associated to the fast switches (<200 ms) and agrees with the measured loading time for UvsW at the working conditions (3 nM), 13 ± 2 s

(measured in an independent experiment). These results demonstrate that the instantaneous switches in the migration direction are not mediated by the binding of new UvsW molecules from solution.

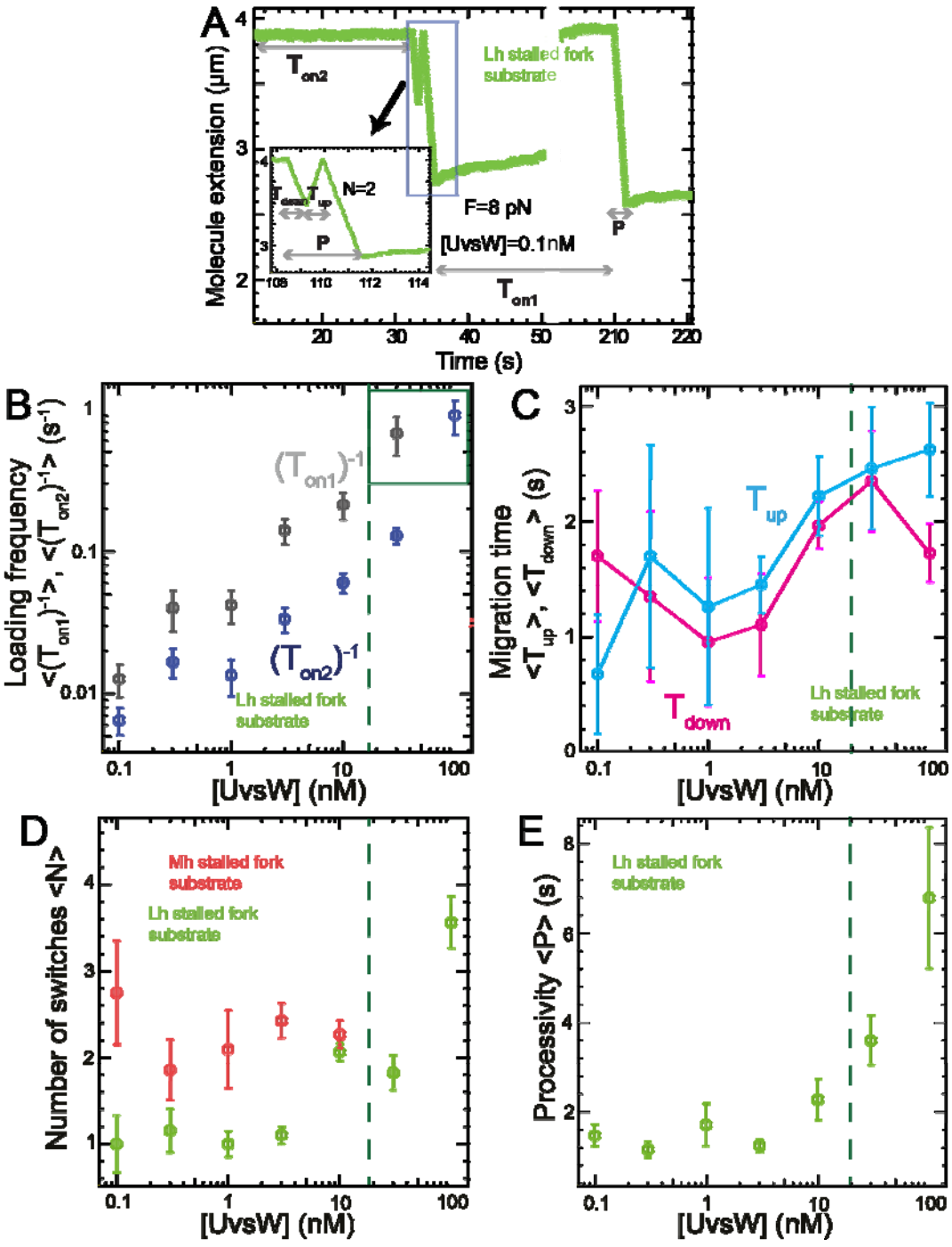

Fig. S12: Instantaneous switches in the branch migration direction mediated by a single UvsW enzyme complex (**A**) Experimental trace showing the molecular extension as a function of time obtained from the HJ migration assays using the Lh stalled fork at F=8 pN in presence of UvsW at 100 pM. (**B**) The inverse of the loading

time of the enzyme T_{on1} (corresponding to the total loading time including loading onto the HJ) and T_{on2} (corresponding to the loading time at the three-way junction fork) as a function of the UvsW concentration. The loading frequency of the enzyme depends linearly with the concentration as expected for a monomeric enzyme. The fact the T_{on1} is much larger than T_{on2} shows that UvsW has a preference for binding a three-way junction as compared to a HJ. On the other hand, one can see that the loading time becomes very short (on the order of seconds) at concentrations above 10 nM. This means that above 10 nM it becomes difficult to distinguish between instantaneous switches and switches involving enzyme dissociation. For the analysis presented here we considered that all switches involving more than 0.5 s where mediated by enzyme dissociation. (**C**) Migration time in downward (T_{down}) and upward (T_{up}) directions before switching as a function of UvsW concentration. Both T_{down} and T_{up} are independent on the concentration. This together with the fact that below 10nM the loading time is much larger than the switching time support the idea that the switching is not generated by the binding of different UvsW complexes from solution because this would give rise to a mean switching time that would decrease with the enzyme concentration. (**D, E**) Average number of switches and average processivity as a function of UvsW concentration. Both <N> and <P> are constant below 10 nM and slightly increase above 10 nM. This increase is an artifact from the high UvsW concentrations where the loading time of the enzyme becomes too short and activity bursts are generated by multiple enzyme binding. Note that the switching frequency is low for the 7 Kbp Lh stalled fork substrate and increases for shorter substrates (red points show the results from the 600 bp Mh stalled fork). Indeed, most of switches on the assays performed with the 600 bp Mh stalled fork substrate occur when the enzyme cannot proceed forward (i.e. when the HJ is totally progressed or regressed, fig. S11). This suggests that *in vivo* UvsW will easily switch direction upon colliding with roadblocks on DNA.

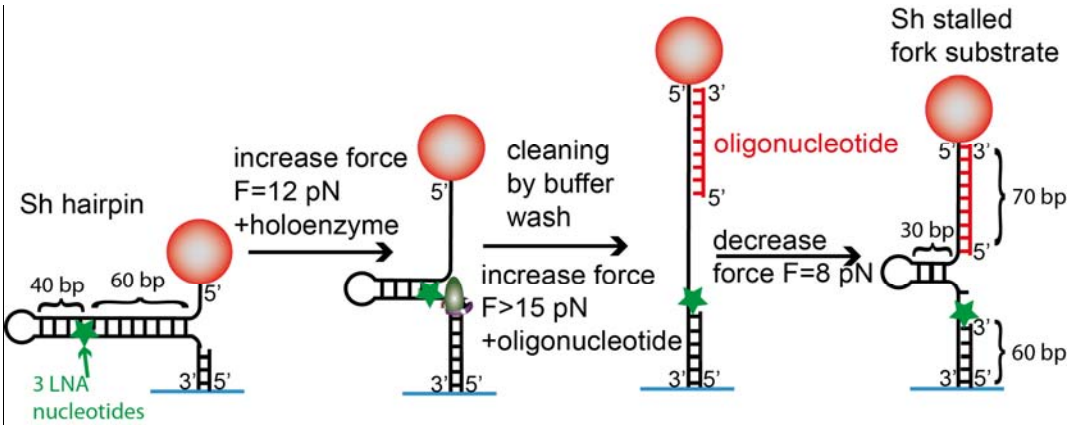

Fig. S13: Stalled fork substrate presenting a lesion on the leading strand. The stalled substrate was generated in situ in the MT reaction chamber. We used the 100 bp hairpin (Sh) with a built-in primer substrate containing three locked nucleic acid (LNA) nucleotides in the template leading strand (40 bp before the apex) presenting an efficient roadblock for the holoenzyme (15). The stalled substrate was generated by first increasing the force to 12 pN to initiate leading strand synthesis by the holoenzyme which extended the primer until reaching the LNA block and next denaturing the hairpin and hybridizing an oligonucleotide complementary to the template lagging strand. The exogenous oligonucleotide mimicking the replicated lagging strand went 10 bases beyond the LNA block. Upon lowering the force a stalled fork-like substrate was generated with the asymmetry needed for initiation of the template switching pathway.

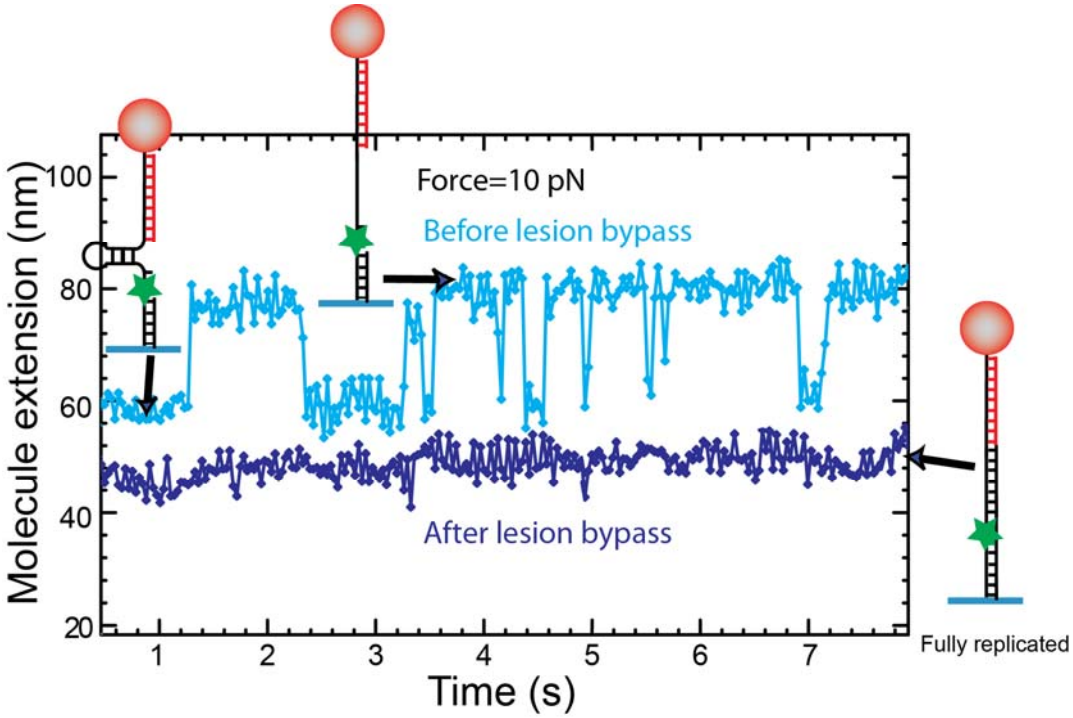

Fig. S14: Testing lesion bypass. Experimental traces showing the extension of the Sh LNA block hairpin as a function of time before (light blue) and after (dark blue) lesion bypass. The traces have been shifted for clarity. The initial substrate was a stalled fork presenting a 40 bp hairpin (trace in light blue). The 40 bp hairpin is AT rich (75% of AT content), and 10 pN was enough to induce its unfolding. Indeed, by applying 10 pN of force the hairpin hopped between the open and close configurations detected as jumps in the measured molecular extension. In contrast, after lesion bypass and final synthesis the substrate was a fully dsDNA molecule and the measured molecular extension did not show the bi-stability associated to the hairpin molecule.

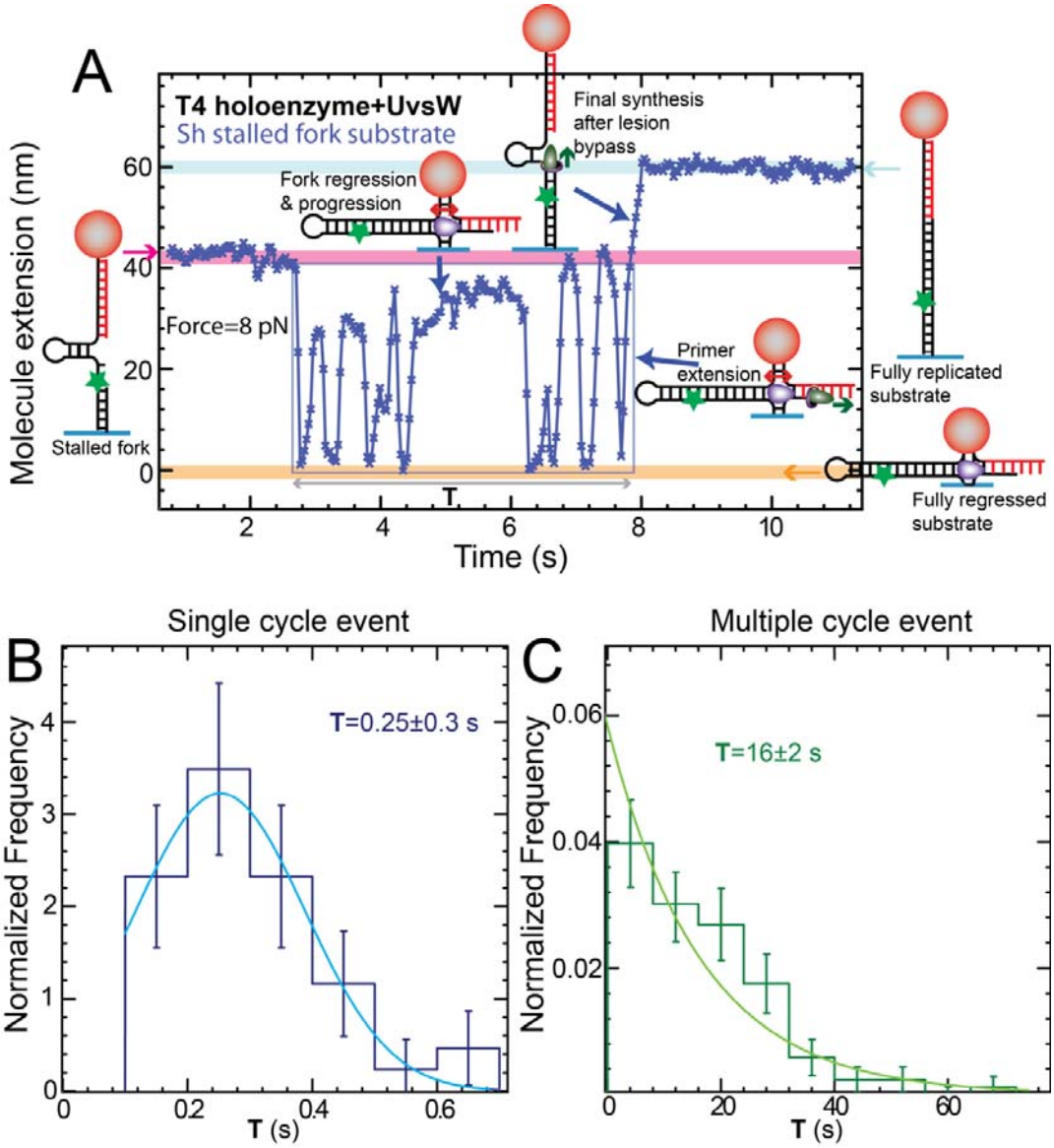

Fig. S15: Lesion bypass by single and multiple cycles of fork regression and progression (**A**) Experimental trace showing the extension of the Sh stalled fork substrate as a function of time obtained in presence of ATP, dNTPs, UvsW and T4 holoenzyme at F=8 pN. Several cycles of fork regression and progression were required before lesion bypass was achieved. This situation probably corresponds to a scenario in which UvsW loaded on the fork before the holoenzyme (see panels B and C). (**B**) Distribution of the characteristic time τ required for lesion bypass measured in events presenting single cycle of fork regression and progression (N=23 events). The fit to a Gaussian function is shown as a continuous line. (**C**) Distribution of the characteristic time τ required for lesion bypass measured in events presenting multiple cycles of fork regression and progression (N=40 events). The fit to an exponential function is shown

as a continuous line. The characteristic time τ for the multiple cycle case (16 s) is close to the measured loading time for the holoenzyme at the working conditions, 22 ± 5 s (measured in an independent experiment), suggesting that multiple cycle events correspond to a scenario in which the UvsW loads first and the holoenzyme is loaded next. The mean number of cycles in the multiple cycle events is 5 ± 2 cycles.

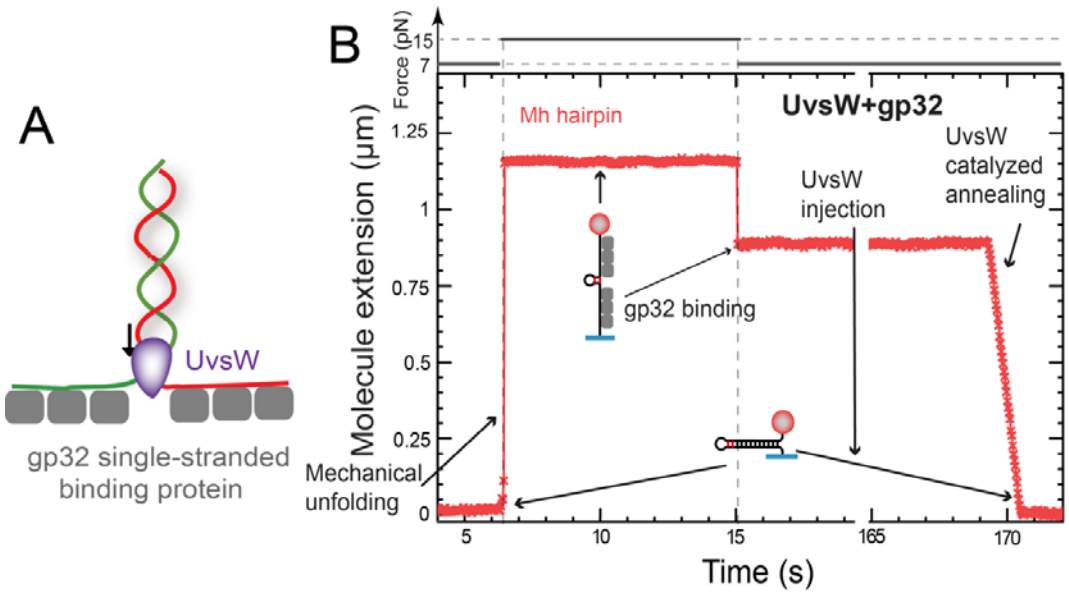

Fig. S16: UvsW-catalyzed protein displacement (**A**) Schematics of the assay. (**B**) Experimental trace obtained from MT annealing assays in presence of gp32 single-stranded DNA binding protein. A large force (15 pN) was first applied generating a partially denatured hairpin with long ssDNA tails. DNA coating was then achieved by injection of the gp32 at high concentrations (300 nM). By decreasing the force to 7 pN the molecule did not refold and presented a fixed extension, a signature of a stable coating. After injection of UvsW and ATP, annealing events were observed. The average annealing rate measured from theses assays was 1200 ± 60 bp/s (N=115 events), close to the measured annealing rate in absence of gp32 (~1300 bp/s).

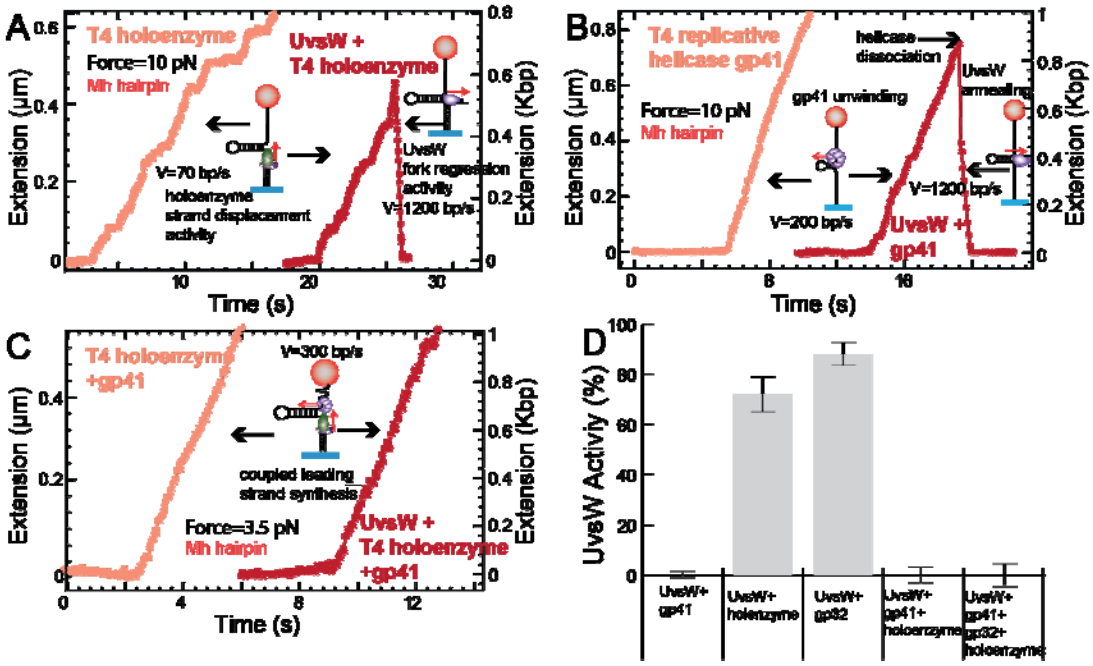

Fig. S17: UvsW activity is inhibited by the replicative helicase but not by the holoenzyme. Experimental traces showing the T4 holoenzyme strand displacement activity (**A**), the gp41 replicative helicase unwinding activity (**B**), and coupled helicase/holoenzyme leading strand synthesis (**C**) on the Mh substrate in absence (light red) and presence (dark red) of UvsW. Both unwinding and synthesis activities were detected as an increase in molecule's extension. The holoenzyme and helicase assays were performed at 10 pN. This force was chosen to be well below the unfolding force (~15 pN) but to be high enough to stimulate both helicase activity and holoenzyme strand displacement activity (28). The helicase/holoenzyme assays were perfomed at a lower force of 3.5 pN because efficient leading strand helicase/holoenzyme coupling is only observed at low forces (below 5 pN) (28). The UvsW was able to load and anneal the fork when the holoenzyme was extending the primer on the leading strand (panel A). In contrast, in presence of gp41 helicase, UvsW activity was only detected after gp41 dissociation (panel B). During the unwinding phase UvsW activity was never detected. In most of the cases, after helicase dissociation the hairpin spontaneously closed without the presence of UvsW annealing burst. Only three events (within ~500 helicase events), showed partial unwinding by gp41 followed by UvsW re-annealing activity (one shown in panel B). Moreover, UvsW activity was totally inhibited in presence of coupled leading strand synthesis where helicase processivity was largely increased (panel C). (**D**) Percentage of traces showing UvsW annealing activity in

presence of different proteins (computed from N=34 to 483 events depending on the protein conditions). Error bars are the SEM.

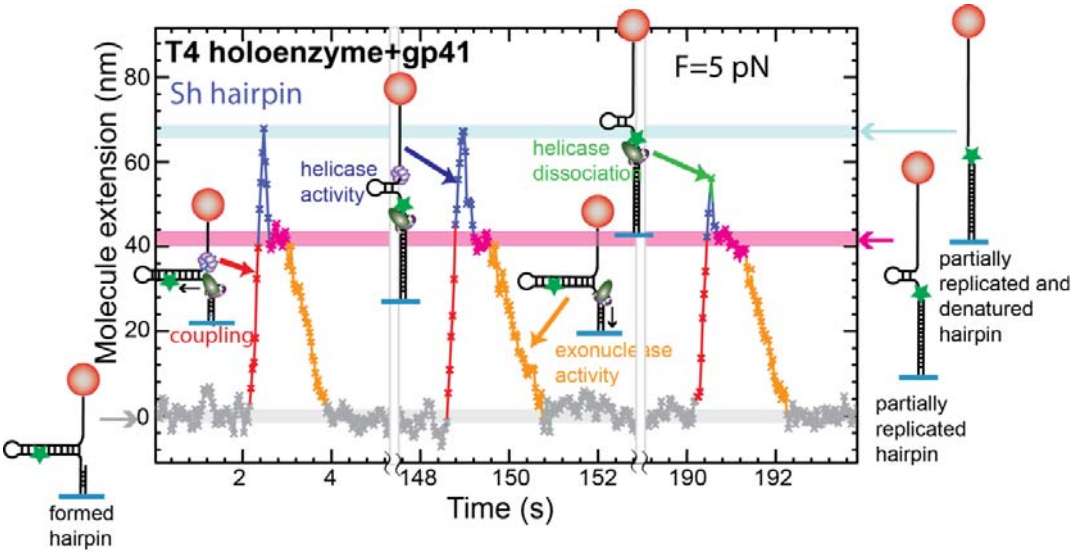

Fig. S18: Helicase and holoenzyme uncoupling at the lesion site. Experimental trace recorded for the T4 holoenzyme and gp41 helicase on the Short 100 bp hairpin (Sh) containing a LNA roadblock 40 bp ahead of the loop apex (fig. S2A). At 5 pN, the holoenzyme alone is inefficient in strand displacement synthesis and the helicase alone is not very processive (28). However, the coupled helicase/holoenzyme system is able to perform efficient leading strand synthesis (28), detected as a fast increase in the molecular extension (red). When the holoenzyme encountered the LNA modified nucleotides on the template strand replication stopped, but the helicase continued unwinding (blue) and dissociated after a short time. In the first two activity bursts the helicase reached the loop apex and then translocated along the ssDNA until it reached the stalled holoenzyme at the LNA block. In the third burst the helicase dissociated before reaching the loop apex (green). After helicase dissociation, the hairpin extension rapidly set back to the position of the LNA lesion because the holoenzyme had synthesized the leading strand until that point (magenta). Since the helicase had disassembled, the fork pushed directly the holoenzyme that was still bound to the LNA block position, which triggered the exonuclease activity (28) and the processive removal of the synthesized strand (yellow).

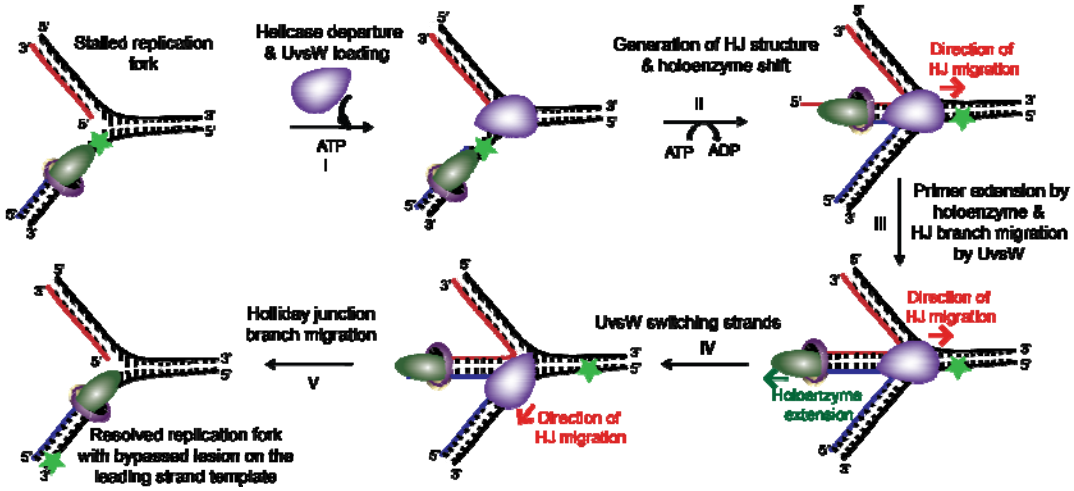

Fig. S19: The template switching pathway in T4 system. The leading strand holoenzyme progression is halted at the lesion site, which causes uncoupled leading and lagging strand synthesis. Uncoupling causes reduction in the unwinding of the duplex DNA by the replicative helicase. (i) Uncoupling leading and lagging strand synthesis slows down the replicative helicase that eventually dissociates from the DNA, after which UvsW loads onto the stalled fork. (ii) The UvsW uses the energy from ATP hydrolysis to regress the fork forming a HJ and shifting the leading strand holoenzyme to the formed HJ. (iii) The holoenzyme then proceeds with leading strand primer extension using the replicated nascent strand from the lagging strand synthesis as the template while UvsW is migrating the HJ. (iv) The UvsW randomly switches direction and (v) progresses the HJ to recover the replication fork where the lesion is now bypassed. The entire process is mediated by a single UvsW molecule.